# Strengthening Mechanism of TiNi Shape Memory Sintered Alloy using Elemental Mixtures of Pre-alloyed TiNi Powder and TiO₂ Particles†

YONEZAWA Takayuki *, YOSHIMURA Tomohiro**, UMEDA Junko***,
KONDOH Katsuyoshi**** , SOUBA Ryouichi*****

**Abstract**

*The mechanical properties and the strengthening mechanism of the extruded and heat-treated titanium-nickel (TiNi) shape memory alloys (SMAs) prepared by powder metallurgy (P/M) were investigated. TiNi pre-alloyed powder was mixed with titanium dioxide (TiO₂) particles by a planetary ball mill, and consolidated by spark plasma sintering (SPS) at a sintering temperature of 1173 K in vacuum (6 Pa). Subsequently, the SPSed TiNi alloy compacts were extruded at a pre-heated temperature of 1373 K, and shape memory heat-treated at a holding temperature of 773 K. Ti₄Ni₂O phases formed by reaction between the TiNi matrix and the additive TiO₂ particles caused an increase of the soluted Ni content of the matrix, and resulted in a decrease of the martensitic transformation temperature of the TiNi matrix. Consequently, the extruded and heat-treated TiNi powder alloy with 1.0 vol.% TiO₂ particles showed a remarkably high plateau stress of 524 MPa and ultimate tensile strength (UTS) of 1298 MPa at room temperature (298 K), respectively. It also revealed a good shape recovery rate of 89.3 % when 8% tensile strain was applied.*

**KEY WORDS: (Shape memory alloys), (Titanium-nickel), (Pre-alloyed powder), (Titanium dioxide), (Powder metallurgy), (Plateau stress)**

## 1. Introduction

Titanium-nickel (TiNi) alloys with near-equiatomic compositions is the most popular shape memory alloy (SMA) with excellent characteristics, such as shape memory effect, superelasticity, high strength, good corrosion resistance and biocompatibility[1)-4)]. Recently, TiNi alloys with superelastic behavior have been used in advanced medical devices, such as guide wire, catheter and stent to restore a damaged blood vessel. In particular, the self-expanding stents using TiNi SMAs are excellent medical devices with a low risk of restenosis. The improvement of mechanical and shape memory properties of the TiNi alloys is effective for reducing the wire diameter of medical devices, and significantly results in a reduction of surgical invasion and an improvement in patients' quality of life (QOL).

TiNi alloys have different phases; the B2 austenite (parent) phase and the monoclinic B19' martensite phase. The superelasticity of TiNi alloys, typically containing 49–51 at.% Ni, can be realized by a stress-induced transformation between B2 parent and B19' martensite phases[4)]. The mechanism of deformation originated in the phase transformation, however, restricts a limitation of the material design for improvement of their mechanical and shape memory properties. Thus, the substantial material design of the TiNi SMAs has been limited by the conventional process such as work hardening, microstructure refinement via plastic deformation and heat treatment[5)-7)].

It is well known that mechanical and shape memory properties of the TiNi alloys are strongly dependent on the soluted Ni and the impurity elements contents of the matrix[4), 8)-10)]. However, the control of the soluted Ni content is difficult by the conventional melting process because of the difference of a specific gravity between Ti (4.51 kg/m³) and Ni (8.91 kg/m³). In addition, the impurity elements may have an adverse effect on biocompatibility. On the other hand, it was reported that

Ti-Ni-O oxides with Ti-rich composition were formed by reaction between TiO$_2$ particles and TiNi alloy and resulted in an increase of the soluted Ni content of the matrix[11]. In general, TiO$_2$ is an oxide formed on the surface of pure Ti, and has an excellent biocompatibility[12]. Therefore, the soluted Ni content of the TiNi alloys is able to be precisely controlled without an adverse effect on biocompatibility by TiO$_2$ additive particles. However, the mechanical and shape memory properties of the TiNi alloys with TiO$_2$ particles have not been investigated in detail. This is because coarse Ti-Ni-O oxides are produced by the conventional melting process, which results in a significant decrease of the ductility of the TiNi alloys[13]. On the other hand, in powder metallurgy process as based on the solid phase, the Ti-Ni-O oxides are able to be uniformly dispersed, and result in the decrease of the adverse effect on the ductility. In the present study, high strength TiNi alloys with TiO$_2$ particles were fabricated by powder metallurgy process, and their microstructural, mechanical and shape memory properties were investigated. The strengthening mechanism of the TiNi alloys with TiO$_2$ particles was discussed by analysis of their microstructures and evaluation of the superelastic behavior in tensile tests.

## 2. Experimental

Ti-51.19 at.% Ni pre-alloyed powder (FUKUDA METAL FOIL & POWDER) having a mean diameter of 58 μm was employed as a starting material in this study. The compositions of the starting powder were as follows; Ni: 51.19, Ti: 48.41, Fe: 0.03, O: 0.20, C: 0.17 (in at.%). The Ti-51.19 at.% Ni alloy has a martensitic transformation temperature below room temperature. Thus, this powder has the B2 parent phase, and shows a superelastic behavior at room temperature. TiO$_2$ particles (KISHIDA CHEMICAL), used as additive particles, were 0.45 μm in mean particle size. The Ti-51.19 at.% Ni pre-alloyed powder with 0, 0.5 and 1.0 vol.% TiO$_2$ particles was prepared by using a planetary ball mill (PULVERISETTE 5, FRITSCH) for a mixing time of 300 min under a mixing speed of 150 rpm. As-premixed powders were consolidated by using a spark plasma sintering (SPS) equipment (SPS-1030, SPS Syntex). The SPS condition was selected as sintering temperature of 1173 K for holding time of 30 min under 40 MPa pressure in vacuum (6 Pa). The diameter of the SPSed billets was 36 mm. The relative densities of the SPSed billets were evaluated by measuring the geometric data and mass of the billets. These SPSed billets were heated to 1373 K and kept 10 min under Ar gas atmosphere by using an infrared gold image furnace (SSA-P610CP, ULVAC-RIKO). The preheated billets were then immediately served to a hot extrusion process using a hydraulic press machine (SHP-200-450, Shibayamakikai) with a ram speed of 6 mm/sec. The extrusion ratio was 6, and the final diameter of the extruded material was 15 mm. In order to improve the shape memory properties, these extruded materials were heat-treated at holding temperature of 773 K for holding time of 60 min by using

a muffle furnace (KDF S-70, Denken), and then water-quenched immediately.

For microstructure observation, specimens were mechanically ground with #400, #1000, and #4000 SiC abrasive papers, and then, polished with 0.3 μm and 0.05 μm Al$_2$O$_3$ polishing suspension. Microstructural observation was carried out by using a field-emission scanning electron microscope (FE-SEM, JSM-6500F, JEOL). The phase compositions in the specimens were identified by X-ray diffraction (XRD, XRD-6100, Shimadzu) and an electron probe microanalyser (EPMA, JXA-8530F, JEOL) equipped by the SEM. The mechanical properties of the extruded and heat-treated (Exted and HTed) specimens were evaluated by conventional tensile tests. The specimens were machined into tensile test pieces with 3 mm diameter and 15 mm gauge length. Tensile tests were performed by using an universal testing machine (Autograph AG-X 50 kN, Shimadzu) with a strain rate of $5 \times 10^{-4}$ s$^{-1}$ at room temperature (298 $\pm$ 2 K). The shape memory properties of the Exted and HTed specimens were evaluated by tensile hysteresis tests. In the tensile hysteresis test, the specimens were loaded 3% and 8% strain, and then, unloaded with a strain rate of $5 \times 10^{-4}$ s$^{-1}$. The shape recovery rate ($R$) was calculated by the following equation:

$$R = \frac{S_T - S_R}{S_T} \times 100 \qquad (1)$$

where $S_T$ and $S_R$ are on set strain and residual strain in the tensile hysteresis test, respectively. The other conditions of the tensile hysteresis test were the same as those of the conventional tensile test.

## 3. Results and Discussion
### 3.1 Microstructure analysis on powder metallurgy TiNi alloys with TiO$_2$

**Figure 1** shows SEM observation of the surface of the TiNi pre-alloyed powder mixed with 1.0 vol.% TiO$_2$ particles. TiO$_2$ particles were uniformly dispersed on the surface of the TiNi pre-alloyed powder by a planetary ball mill. Their segregation was not confirmed. SEM microstructural observation and relative densities ($\rho_R$) of the SPSed TiNi compacts with 0~1.0 vol.% TiO$_2$ particles (X-TiO$_2$ composite; X = 0, 0.5, 1.0) are shown in **Fig. 2**. In each specimen, pores were detected at the tri-junction points of the primary powders. The relative density was about 95%, respectively. The compound phases existed at the primary powder boundaries of
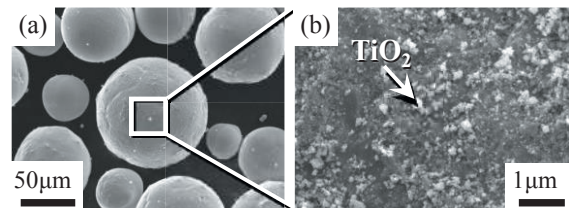


**Fig. 1** SEM observation on TiNi alloy powder mixed with 1.0 vol.% TiO$_2$ particles; (a) low magnification and (b) high magnification.

SPSed 0.5-TiO$_2$, 1.0-TiO$_2$ composites. EPMA map analysis on the primary powder boundaries of the SPSed 1.0-TiO$_2$ composite is shown in **Fig. 3**. The compound phases had Ti and O-rich composition. In addition, diffraction peaks of Ti$_4$Ni$_2$O phase were detected by XRD analysis for the SPSed 0.5-TiO$_2$, 1.0-TiO$_2$ composites, and their intensities increased with an increase of additive TiO$_2$ content. So these compound phases were identified as Ti$_4$Ni$_2$O phase. Ti$_4$Ni$_2$O formed by reaction between TiO$_2$ and TiNi is an oxide which is

much thermodynamically stable compared to TiO$_2$[12), 13)]. The volume fraction of Ti$_4$Ni$_2$O phase of the SPSed 1.0-TiO$_2$ composite by image analysis of SEM image was 6.82 vol.%, which was similar to that of Ti$_4$Ni$_2$O phase calculated from the total oxygen content in the SPSed compact. In addition, the TiO$_2$ additive particles were not detected in the SPSed 0.5-TiO$_2$, 1.0-TiO$_2$ composites. Therefore, the Ti$_4$Ni$_2$O phases at the primary powder boundaries were formed during SPS by reaction between the TiNi matrix and the TiO$_2$ additive particles. On the
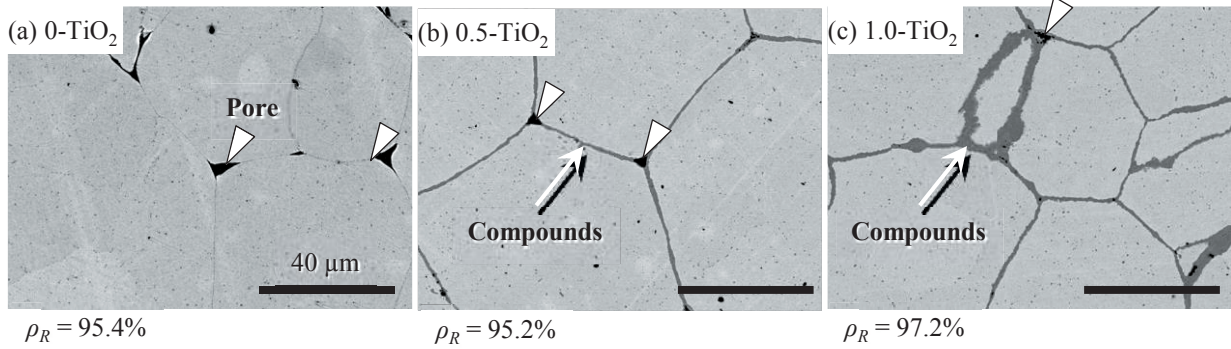
(a) 0-TiO$_2$

**Pore**

40 µm

$\rho_R$ = 95.4%

(b) 0.5-TiO$_2$

**Compounds**

$\rho_R$ = 95.2%

(c) 1.0-TiO$_2$

**Compounds**

$\rho_R$ = 97.2%

**Fig. 2**   SEM observation on SPSed X-TiO$_2$ composites (a) ~ (c).

COMPO

Ti

CP        10 um

Ti        10 um

Ni

O

Ni        10 um
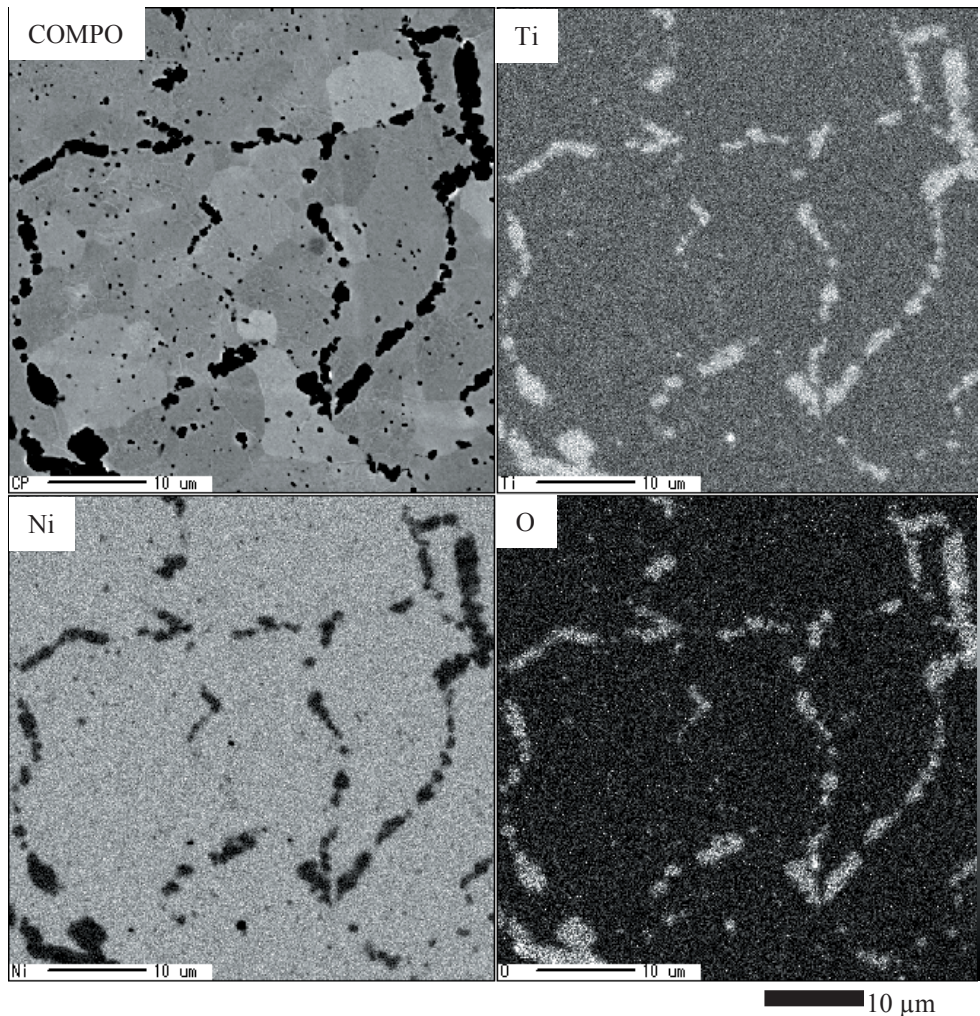
O        10 um

10 µm

**Fig. 3**   EPMA map analysis on primary powder boundaries of SPSed 1.0-TiO$_2$ composite.

other hand, the soluted Ni content of the matrix was increased by the formation of $Ti_4Ni_2O$ phase with Ti-rich composition. The revised solid solubility of Ni ($[Ni_R]$) by consideration of the composition changes in the formation of $Ti_4Ni_2O$ phase was calculated by the following equation[13]:

$$[Ni_R] = \frac{[Ni] - 2[O]}{100 - 7[O]} \times 100 \qquad (2)$$

where [Ni] and [O] are the total Ni and O content of the SPSed compacts, respectively. From this equation, the amount of the increment of the soluted Ni content of the SPSed 0.5-TiO₂, 1.0-TiO₂ composites were 0.38 at.%, 0.78 at.%, respectively.

SEM microstructures of the Exted and HTed X-TiO₂ composites (a) ~ (c) are shown in **Fig. 4**. The Exted and HTed specimens had dense microstructures without a void. $Ti_4Ni_2O$ phases formed at the primary powder boundaries were dispersed parallel to the extrusion direction by hot extrusion (as shown in Fig.4 (b) ~ (c)). In addition, there was no crack and void at the interface between the TiNi matrix and the $Ti_4Ni_2O$ phases, and this indicates the coherency of interface was good.

### 3.1 Mechanical and shape memory properties of TiNi alloy composites with TiO₂

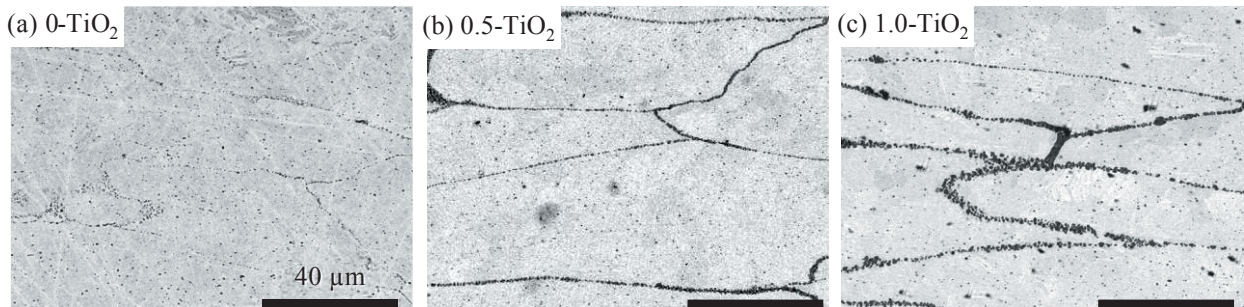**Figure 5** shows the nominal stress versus nominal strain curves of the Exted and HTed X-TiO₂ composites evaluated by the conventional tensile test (a) and tensile hysteresis test (b) at room temperature. The average values of the plateau stress, the ultimate tensile strength (UTS), the elongation, and the shape recovery rates are summarized in **Table 1**. The shape recovery rates in the tensile hysteresis tests were calculated by Equation (1). The mechanical properties of the Exted and HTed X-TiO₂ composites were improved by the increase of the additive TiO₂ content while the suitable ductility was obtained. In particular, the 1.0-TiO₂ composite showed a high plateau stress of 524 MPa and UTS of 1298 MPa, which were 61.7% and 23.1% higher compared to the monolithic TiNi alloy with no TiO₂ particles. In addition, the 0.5-TiO₂ and 1.0-TiO₂ composites showed good shape recovery rates of about 90% when 8% strain was given to the specimens.

As mentioned above, the mechanical and shape memory properties of the TiNi alloys are strongly dependent on the soluted Ni content[4]. Then, the relationship between the increment of the soluted Ni content and the increment of plateau stress was theoretically calculated. In TiNi alloys with near-equiatomic compositions, the martensitic transformation ($M_S$) temperature has a negative correlation with an increase in the soluted Ni content[4].

(a) 0-TiO₂ (b) 0.5-TiO₂ (c) 1.0-TiO₂



40 μm

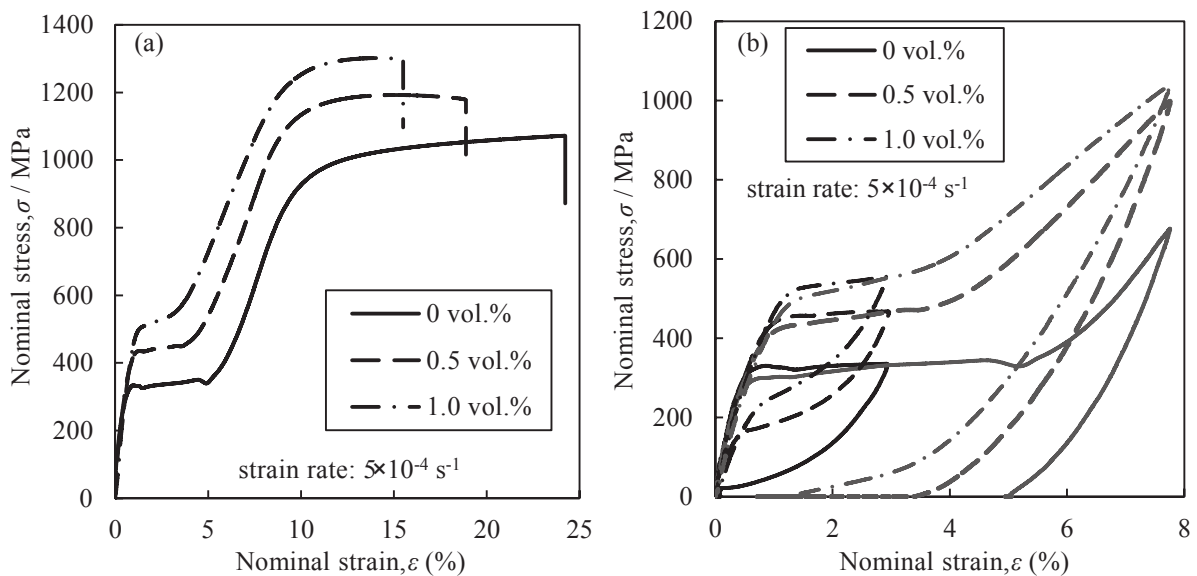**Fig. 4** SEM observation on Exted and HTed X-TiO₂ composites (a) ~ (c).



**Fig. 5** Tensile behavior of Exted and HTed X-TiO₂ composites in tensile test (a) and tensile hysteresis test (b).

**Table 1** Mechanical and shape memory properties of Exted and HTed X-TiO$_2$ composites.

| | Plateau Stress | UTS | Elongation | Shape recovery rate (%) | |
| --- | --- | --- | --- | --- | --- |
| | MPa | MPa | % | $S_T = 3\%$ | $S_T = 8\%$ |
| 0 vol.%TiO$_2$ | 324 | 1054 | 26.3 | 100 | 38.3 |
| 0.5 vol.%TiO$_2$ | 444 | 1205 | 18.9 | 100 | 91.3 |
| 1.0 vol.%TiO$_2$ | 524 | 1298 | 15.2 | 98.1 | 89.3 |

As a result, the amount of $M_S$ temperature change per unit soluted Ni content shows -85.4 K/at.% Ni[13]. On the other hand, from the relationship between the Gibbs free energy of the parent phase and the martensite phase, the relationship between the amount of plateau stress change ($\Delta\sigma_P$) and that of $M_S$ temperature change ($\Delta M_S$) is calculated by the following equation[14]:

$$\Delta\sigma_p = \frac{\Delta S}{\gamma V_M}\Delta M_S \qquad (3)$$

where $\Delta S$, $\gamma$ and $V_M$ are transformation entropy, transformation strain and molecular volume of the TiNi alloys, respectively. In this study, $\Delta S/\gamma V_M$ was set as -3.03 MPa/K [4), 15)]. From Equation (3), the amount of the increment of plateau stress per unit soluted Ni content was calculated as 256 MPa/at.% Ni. **Figure 6** shows the relationship between the revised soluted Ni content calculated by Equation (2) and the plateau stress of the Exted and HTed X-TiO$_2$ composites. The increasing rate of these plots was 253 MPa/at.% Ni, which was almost the same value calculated by Equation (3). Therefore, the strengthening mechanism of plateau stress of the TiNi alloys with TiO$_2$ particles was due to the increase of the soluted Ni content of the matrix by the formation of Ti$_4$Ni$_2$O phase with Ti-rich composition.
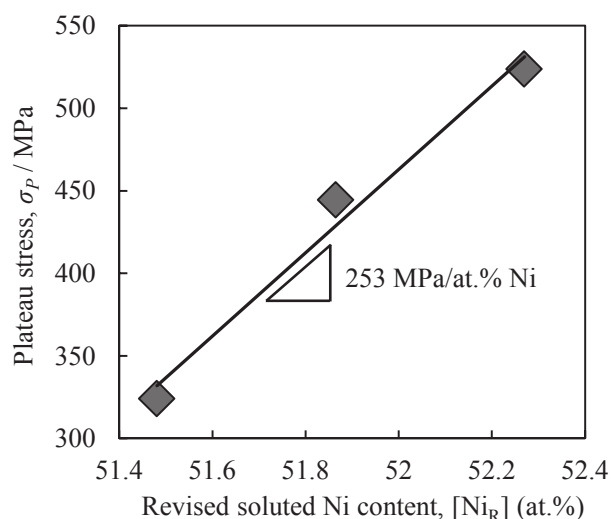


**Fig. 6** Relationship between revised soluted Ni content of TiNi matrix and plateau stress of Exted and HTed X-TiO$_2$ composites.

## 4. Conclusions

In this study, the mechanical properties and the strengthening mechanism of the TiNi alloys with TiO$_2$ particles by powder metallurgy were investigated. The soluted Ni content of the matrix was increased by the formation of Ti$_4$Ni$_2$O phase. The Exted and HTed TiNi specimen with 1.0 vol.% TiO$_2$ particles showed a high plateau stress of 524 MPa, UTS of 1298 MPa, elongation of 15.2%, and a good shape memory rate of 89.3 % when 8% strain in tensile was applied. The main strengthening mechanism of the TiNi alloys with TiO$_2$ particles was a decrease of the $M_S$ temperature by the increase of the soluted Ni content of the matrix.

**Reference**
1) K. Takeda, H. Tobushi, K. Miyamoto, E. A. Pieczyska, Materials Transactions, Vol. 53 (2012) pp. 217-223.
2) J. K. Allafi, B. A. Ahmadi, M. Zare, Materials Science and Engineering: C, Vol. 30 (2010) pp. 1112-1117.
3) P. Filip, J. Lausmaa, J. Musialek, K. Mazanec, Biomaterials, Vol. 22 (2001) pp. 2131-2138.
4) K. Otsuka, X. Ren, Progress in Materials Science, Vol. 50 (2005) pp. 511-678.
5) Y. Zheng, F. Jiang, L. Li, H. Yang, Y. Liu, Acta Materialia, Vol. 56 (2008) pp. 736-745.
6) D. Vojtěcha, M. Voděrováa, J. Kubáseka, P. Nováka, P. Šedáa, A. Michalcováa, J. Fojta, O. Mestekc, Materials Science and Engineering: A, Vol. 528 (2011) pp. 1864-1876.
7) V. G. Pushina, V. V. Stolyarovb, R. Z. Valievb, T. C. Lowec, Y. T. Zhu, Materials Science and Engineering: A, Vol. 410-411 (2005) pp. 386-389.
8) T. H. Nam, D. W. Chung, J. S. Kim, S. B. Kang, Materials Letters, Vol. 52 (2002) pp.234-239.
9) S. K. Wu, H. C. Lin, T. Y. Lin, Materials Science and Engineering: A, Vol. 438-440 (2006) pp. 536-539.
10) H. C. Lina, K. M. Lina, S. K. Changa, C. S. Linb, Journal of Alloys and Compounds, Vol. 284 (1999) pp. 213-217.
11) V. G. Chuprina, I. M. Shalya, Powder Metallurgy and Metal Ceramics, Vol. 41 (2002) pp. 85-89.
12) W. E. Yanga, H. H. Huang, Thin Solid Films, Vol. 518 (2010) pp. 7545-7550.
13) Y. Shugo, S. Hanada, T. Honma, Bulletin of the Research Institute of Mineral Dressing and Metallurgy, Vol.41 (1985) pp. 23-34.
14) M. Kato, H. R. Pak, Physica status solidi (b), Vol. 123 (1984) pp. 415-424.
15) W. Tang, Metallurgical and materials transactions: A, Vol.28 (1997) pp. 537-544.